Garaba, S.P.; Voss, D.; Wollschlaeger, J.; Zielinski, O.:

Modern approaches to shipborne ocean color remote sensing

In: Applied Optics (2015) Optical Society of America

DOI: 10.1364/AO.54.003602

Modern approaches to shipborne ocean color remote sensing

Shungudzemwoyo P. Garaba [1,*], Daniela Voß [1], Jochen Wollschläger [2] and Oliver Zielinski [1]

[1]Institute for Chemistry and Biology of the Marine Environment - Terramare, Carl von Ossietzky University of Oldenburg, Schleusenstraße 1, 26382 Wilhelmshaven, Germany

[2]Institute for Coastal Research, Helmholtz-Zentrum Geesthacht, Max-Planck-Straße 1, 21502 Geesthacht

*Corresponding author: shungu.garaba@uni-oldenburg.de

In this work, modernized shipborne ocean color remote sensing procedures are discussed. For collection of high resolution radiometric quantities a setup of five radiometers and a bidirectional camera system, providing panoramic sea surface and sky images, is proposed. Visual inspection of camera images is utilized as a supporting qualitative verification tool for measured radiometric quantities before calculating ocean color products e.g. water leaving radiance and remote sensing reflectance (R_{RS}). A peak around R_{RS} (760 nm) was observed in spectra affected by relatively high surface reflected glint (SRG) which suggests this waveband could be a useful SRG indicator. Simplified steps applicable to computing uncertainties in SRG corrected R_{RS} are proposed and discussed. The possibility of utilizing 'un-weighted multi-model averaging' to determine the 'best approximation R_{RS}', which is the average of four or more common SRG correction models is examined. This 'best approximation R_{RS}' provides an estimate of R_{RS} based on assumptions derived from several radiative transfer simulations and field investigations. It is important to consider that, applying the average R_{RS} strongly depends on user needs such as spectra intensity, shape, or band ratio in inferring optically active water constituents. However, applying the average R_{RS} is anticipated to mitigate the uncertainties or biases that result from user inherent subjective choice of a particular SRG correction model. Comparisons between in-water and above-water observations are used to assess the extent of applicability of SRG multi-model averaging. Correlations among standard SRG models were tested to determine degree of association or similarities in the SRG models. It is suggested that uncertainty in the 'best approximation R_{RS}' be determined by the unbiased percent difference between the highest and the lowest SRG corrected R_{RS} from the four or widely used approaches. Findings and proposals in this work are aimed at contributing towards uniform and traceable methodology to determine shipborne R_{RS} and its errors to ensure comparability with future investigations. The ocean color community is also encouraged to publish radiometric field measurements with matching metadata in open access databases.

1.Introduction

Remote sensing reflectance (R_{RS}) is an important ocean color remote sensing end-product used to infer optically active water constituents linked to climate change which has seen it gain the name essential climate variable (GCOS, 2011; IOCCG, 2008). To determine R_{RS} Eq. (1) is widely implemented

$$R_{RS} = \frac{L_T - L_{SR}}{E_D} = \frac{L_T - (\rho \times L_{sky} + R)}{E_D} \quad (1)$$

where $L_T(\theta_T, \Phi, \lambda)$ is the total upwelling sea surface radiance, $E_D(\lambda)$ is total downwelling irradiance, L_{sky} is the sky leaving radiance and $L_{SR}(\theta, \Phi, \lambda)$ is the surface reflected glint (SRG). L_{SR} consists of a fraction ($\rho \approx 0.02 - 0.05$) of the sky reflected light and R which is an approximation of sun glint, residual glint, whitecaps, and foam reflected light (Garaba and Zielinski, 2013c; Moore, 1980; Olszewski and Darecki, 1999; Yan and Sydor, 2006). At present it is not possible fully quantify all components of L_{SR} especially R however most SRG approaches are assumed to provide a best approximate of R_{RS}.

Handling of SRG in shipborne ocean color remote sensing is rather naturally subjective, as no correction method has been widely preferred in all water bodies (Garaba and Zielinski, 2013c; Hooker et al., 2002). The absence of a standard SRG technique to determine corrected radiometric quantities makes it very challenging to compare observations from numerous shipborne remote sensing studies. The problems in comparing observations arise from different investigations using various (i) sensor geometry i.e. nadir-zenith angle and relative azimuthal angle of sensors to the sun, (ii) little or no available/recorded additional important information about sea state and cloud conditions, (iii) optical sensor sensitivity as well as traceable calibration of sensors, and (iv) observations during non-optimal sea and sky conditions (Garaba and Zielinski, 2013c; Hooker et al., 2002; Lee et al., 2014). Issues (i) and (ii) are steps well defined in standard protocols for shipborne remote sensing (Mobley, 1999; Mueller et al., 2003; Toole et al., 2000). Despite all these recommended steps, some shipborne remote sensing investigations seem not to report the metadata as they do not record the metadata or maybe record the metadata but do not report the metadata in their work. Furthermore, the SRG correction approaches widely used were developed using a rather limited set of in-situ observations and thus tend to rely on assumptions that might not accurately represent the field observations from different regions and environmental conditions (Garaba and Zielinski, 2013c). For these reasons, there is a likelihood of errors and uncertainties that needs to be traceable and verified in ocean color remote sensing.

Additional steps have also been proposed to mitigate the effects of SRG or L_{SR} contamination in shipborne remote sensing such as (i) collecting measurements at azimuthal angles 90 - 135 ° relative to the sun aimed at reducing possible contamination from ship shadow (Mueller et al., 2003), (ii) directly

measuring water leaving radiance just below the sea surface at over the side stations with domed cover attached to a radiance radiometer which eliminates the need for SRG correction (Tanaka et al., 2006), (iii) profiling light within the water column and extrapolating the measured quantities to the sea surface at over the side stations (Hooker et al., 2002), (iv) polarization techniques (Fougnie et al., 1999; Harmel et al., 2012; Yan and Sydor, 2006) and (v) statistical time series analysis of measurements (Olszewski and Kowalczuk, 2000). Despite all these proposed techniques, the ocean color community still endeavors to reach a common approach. Among the hurdles are instrument costs and availability, lack of uncertainty analysis, shipborne time, and expertise of persons obtaining measurements.

One technique that has not been fully utilized in ocean color SRG correction models is the use of multi-model averaging. Multi-model averaging has been used to predict variables both in social and natural sciences predictive models for decades (Barnard, 1963; Hoeting et al., 1999; Nakagawa and Freckleton, 2011). Moreover, statisticians suggest that multi-model averaging improves uncertainty analysis like biases and minimizes the risk of overconfident conclusions arising from using a single model (Draper, 1995; Hodges, 1987; Hoeting et al., 1999). Applying the multi-model average also benefits from the fact that all the SRG correction models are based on near homogenous assumptions used in radiative transfer simulations (e.g. wind speed, cloud cover, cloud type, optically active water components, light distribution, sensor geometry) theories as well as field observations that tend to overlap and therefore share some consistencies as explained in detail by a recent review (Garaba and Zielinski, 2013c). These scenarios and the extent of overlap are in a way similar to those found in e.g. Intergovernmental Panel on Climate Change models which makes multi-model averaging in determining ocean color products suitable. However, it is also important that users take care when applying the average R_{RS} as it might affect their bio-optical algorithms which might depend on spectra shape, intensity or band ratio.

In this work we aim to expand on a recent review on methods of reducing SRG in shipborne remote sensing (Garaba and Zielinski, 2013c), by proposing modern approaches with special focus on uncertainty analysis that can be easily implemented in shipborne ocean color remote sensing observations. The possibility of multi-model averaging of standard SRG correction models is examined and discussed using sample field measurements. Part of this study is to contribute towards a growing need for a common generic SRG approach to determine R_{RS} and its associated uncertainties, for instance there is an increasing number of investigations related to understanding ocean color product similarities, dependencies, and uncertainties (de Moraes Rudorff et al., 2014; Lee et al., 2014; Wang et al., 2005). Additionally, an improved sensor setup is proposed and its suitability in future shipborne ocean color remote sensing is discussed.

2. Data and methods

2.1 Camera system and radiometer setup

To collect panoramic sea surface and sky images a commercially available security camera Mobotix DualDome D12 equipped with two L43 lenses with 45° horizontal perspective is used. The system is fixed at the ships rail directly above the bridge room (Fig. 1). With the new setup the camera provides a near panoramic view of the sea and sky. Acquisition of images is synchronized with the radiometer measurements. A set of 5 TriOS RAMSES radiometers is implemented at the top of the foremast; one ACC hyperspectral cosine irradiance meter and four ARC hyperspectral radiance meters with 7° field-of-view in air. The RAMSES-ACC hyperspectral cosine irradiance meter is used to measure the total downwelling irradiance E_D (λ). Two RAMSES-ARC meters are positioned at a nadir angle of 45 ° facing the sea surface to measure the total upwelling sea surface radiance $L_T(\theta_T, \Phi, \lambda)$ with a relative azimuthal angle between them of 90 °. The other two RAMSES-ARC meters with same relative azimuthal angle of 90°, are positioned at a zenith angle of 45 ° facing the sky to measure the sky leaving radiance $L_{sky}(\theta_{sky}, \Phi, \lambda)$. A more detailed schematic of the radiometer platform is shown in Fig. 2.

2.2 Beam attenuation and absorption measurements

Underway measurements of beam attenuation and absorption coefficient of sample water were performed using a WETlabs AC-9 meter in flow-through mode. Sample water from a depth of about 4 m was continuously pumped through a custom made Pocket-FerryBox (4H-Jena, Germany) which measured standard oceanographic parameters (practical salinity, temperature, chl-*a* fluorescence) and passed on to the AC-9.

Beam attenuation and absorption coefficient measurement were filtered using a running median to eliminate effects of bubbles. The measurements were corrected for temperature and salinity effects using the data obtained with the FerryBox-system and the coefficients published in Pegau et al. (1997). Instrument calibration was carried out at regular intervals using purified water. To account for light scattering effects, the absorption data were corrected using a modern approach (Röttgers et al., 2013). By visual inspection of the data, one of the absorption channels (630 nm) provided measurements which were qualitatively reasonable but relatively too high with respects to the other neighboring channels. For this reason, the data of this channel were omitted from the analysis. Beam attenuation and absorption coefficients were converted into above water remote sensing reflectance (R_{rs}) using Eq. (2)

$$R_{rs} = T \times \frac{f}{Q} \times \frac{b_{Total}}{a_{Total} + b_{Total}} \quad (2)$$

Where T = 0.52 is the reflection and refraction components of the water surface and f/Q = 0.13 is the bidirectional component of light (Loisel and Morel, 2001). The AC-9 bandwidth data is centered over a 10 nm window and therefore the above water R_{RS} is also centered to match this bandwidth.

2.2 Calculating R_{RS} uncertainty

A revised protocol and review of SRG correction models suggests the use of several approaches. It proposes a set of objective steps for selecting an appropriate correction (Garaba and Zielinski, 2013c). To determine the best R_{RS} this selection can be tedious and does not provide any uncertainties in the end product R_{RS}. We therefore suggest obtaining uncertainty in R_{RS} [sr^{-1}] at distinct wavelengths by using unbiased percent difference (*UPD*) in Eq. (2)

$$UPD[\%] = \frac{|X_{\min} - X_{\max}|}{0.5 \times (X_{\min} + X_{\max})} \times 100 \qquad (2)$$

where $X_{\max}$ is the highest R_{RS} spectra and $X_{\min}$ is the lowest R_{RS} spectra after SRG correction. *UPD* provides the uncertainty between two observations from which the correct one is unknown. Use of *UPD* is considered appropriate here because it provides an unbiased comparison quantification of the difference between the least corrected – highest signal and most corrected – lowest signal. Furthermore, *UPD* provides a relative uncertainty or error comparison quantity that has been used for both practical and theoretical applications in social and natural sciences (Makridakis, 1993).

To apply this statistical parameter to remote sensing, the R_{RS} is determined by the four main surface reflected glint correction models (Gould et al., 2001; Lee et al., 2010; Mobley, 1999; Ruddick et al., 2006). Hereon these models will be referred to as M99, G01, R06, and L10; the first letter represents the author and the year of publication. To mitigate the challenge that arise from subjectivity or justifying use of a particular approach as reported (Garaba et al., 2014a; Garaba et al., 2014b; Garaba and Zielinski, 2013a), the multi-model average of these four approaches will therefore be the 'best approximation R_{RS}' reported as in Eq. (3)

$$R_{RS}[sr^{-1}] \Rightarrow X_{mean}\left(X_{\min}, X_{\max}\right) \qquad (3)$$

where X_{mean} is the multi-model average R_{RS}, X_{min} is the minimum and X_{max} is the maximum R_{RS} determined by one of the four models. Therefore the uncertainty at a particular wavelength 'best approximation R_{RS}' is the *UPD* computed in Eq. (2). An additional parameter to determine the maximum error (ΔX_{max}) will be evaluated using Eq. (4),

$$\Delta X_{\max}[sr^{-1}] = 0.5 \times \left(X_{\max} - X_{\min} \right) \Rightarrow X_{mean} \pm \Delta X_{\max} \quad (4)$$

Uncertainty between above-water and in-water derive R_{RS} (X) was computed from mean absolute percent difference (*MAPD*) and mean percent difference (*MPD*). *MAPD* Eq. (5) and *MPD* from Eq. (6) are measures of scatter and bias respectively.

$$MAPD[\%] = 100 * \frac{1}{N} \sum_{i=1}^{N} \frac{\left| X_{above-water} - X_{in-water} \right|}{X_{in-water}} \quad (5)$$

$$MPD[\%] = 100 * \frac{1}{N} \sum_{i=1}^{N} \frac{X_{above-water} - X_{in-water}}{X_{in-water}} \quad (6)$$

3. Results and discussion

3.1 Camera and spectra features

Onboard R/V Heincke the new camera system provides a near panoramic view of the sea surface and sky region matching the radiometric observations. The radiometers are located at the top of the foremast directly in front of the camera system. The goal of taking radiometric measurements at azimuthal angles of 90 - 135 ° relative to the sun is to reduce the surface reflected glint contamination. Based on our camera image inspection, at any time the azimuthal angle between the sea surface facing radiometers guarantees that one of the radiometers is at least targeted at a sea surface region with little or minimal visible glitter. An example of images with calculated R_{RS} spectra are shown in Fig. 3. The apparent glint or glitter is observed in the right (starboard) image of Fig. 3, little or minimal visible glitter can be observed in the left (portside) image. Corresponding calculated R_{RS} spectra on the right (starboard) side is relatively high over the measured spectrum based on the SGR by M99 and R06. It is however high only in the green spectrum and around 760 nm for the SGR corrected spectra by G01 and L10. To examine this we look at the correlations in the next section.

A unique feature was observed in all spectra and is highlighted (Fig. 4). At the R_{RS} wavelength range 750 – 780 nm it was noted that in the presence of sun glitter there is a peak right (starboard) side while in the absence of glitter the signal is nearly flat left (portside). These wavebands around 760 nm have been shown to be associated with oxygen absorption and to some degree related to glint (Kutser et al., 2009). In this work we presume that this feature might be an artifact or could also be attributed to a characteristic of the oxygen signature that is related to surface reflected glint. It is proposed that more work should consider this band as a proxy for sunglint presence.

3.2 Negative R_{RS}

The aspect of negative R_{RS} spectra is of major concern in the ocean color community (Garaba and Zielinski, 2013c; Olszewski and Darecki, 1999; Yan and Sydor, 2006). In a case study sources of negative spectra were investigated and found out that the negative spectra arise from assuming a flat water surface or using Fresnel reflectance in SRG correction (Yan and Sydor, 2006). Yan and Sydor (Yan and Sydor, 2006) further illustrate the influence of colored dissolved organic material in approximating R_{RS} which can lead to false negative values. In their work they also suggest that waters with back scattering coefficient : absorption coefficient of yellow substance at 400 nm less than 1 will produce negative R_{RS}. The root cause of negative spectra lies in the SRG correction, therefore users ought to be careful when applying any particular correction method. In most cases when you have negative values in G01 you are likely to have negative values in L10 because these two models assume Fresnel reflectance but they slightly vary in the magnitude of residual glint they generate. The M99 use a reflectance factor of 0.028 whilst R06 varies depending on cloud cover and wind speed. It is recommended to omit negative values in any ocean color information analysis.

3.3 Uncertainties at individual wavebands and band ratio

Goals of this section are to compare the different surface reflected correction models and evaluate the use of the multi model R_{RS}, we look at the R_{RS} at 440, 488, 555, 676 and 730 nm as well as the band ratio 488/555 nm. These wavebands are widely used in classic predictive algorithms and for comparison tasks (de Moraes Rudorff et al., 2014; Garaba et al., 2014b; Garaba and Zielinski, 2013a; Wang et al., 2005). A total of 943 above-water and in-water measurements were collected underway in the North Sea aboard R/V Sonne in September 2014. These measurements were matched according to time of measurement. Above-water measurements were collected at 5 minute intervals whilst the in-water at 1 minute intervals. In-water AC-9 information was then averaged to ± 2 minutes matching the above-water information. Uncertainties in the measurements (Table 1) were determined using Eq. (5) and Eq. (6).

At each wavelength investigated in Table 1 it is observed that the bias and scatter of SRG corrected information is variable. For example at 440 nm L10 provides minimal bias or MPD (3 ± 47) % but at 488 nm G01 provides better statistics MPD (0 ± 42) % and for the band ratio 488/555 the average of all models provides better statistics. Based on our dataset when applying band ratio the average of SRG corrected spectra has minimal uncertainties but at individual wavebands each SRG model has varying uncertainties relative to in-water observations. Average bias or MPD was generally less than 25 % and scatter MAPD was less than 50 %. We assume these are moderate uncertainties for underway observations considering that environmental perturbations arise from rough sea surface conditions, wind speed and cloud cover.

3.4 Correlation tests among SRG models

We applied Spearman's rank-order correlation test to determine the degree of association among the models. Spearman's rank-order correlation test was applied because the dataset was determined to be of non-normal distribution based on Shapiro-Wilk's parametric hypothesis test. A total of 2152 measurements from high latitude melt waters and fjordal waters as well as northwestern European shelf seas were analyzed here. These observations are available on request and some are available in open access form via the PANGAEA online database (Garaba et al., 2011; Garaba and Zielinski, 2013b). For brevity we only check for Spearman correlations in the blue (440 nm) Fig. 5, green (555 nm) Fig. 6, red (715 nm) Fig. 7 and the band ratio (490/555 nm) Fig. 8. Negative values are eliminated in the analysis stage and in MathWorks Matlab 2014a they are set to NaN. Spearman correlation statistics are presented in Fig. 5 – Fig. 8.

Spearman correlations in the blue spectrum at 440 nm show that all SRG models excluding the average had very weak to very strong positive significant associations among themselves, whilst average of the SRG models had moderate to very strong significant associations with all models. The green spectrum at 555 nm show that all SRG models excluding the average had weak to very strong positive significant associations among themselves, whilst average of the SRG models had strong to very strong significant associations with all models. The red spectrum at 715 nm show that all SRG models excluding the average had very weak to very strong positive significant associations among themselves, whilst average of the SRG models had moderate to very strong significant associations with all models. Band ratio (490/555) nm had in general very strong significant associations for all SRG models and the average of these models. These correlation statistics suggest that the SRG models tested here share some statistically significant similarities of varying degrees of association, with very strong significant correlations between G01 and L10 as well as M99 and R06. The positive significant associations determined here are consistent with our assumption, the SRG correction models are based on common assumptions used in radiative transfer simulations, theories as well as field observations that tend to overlap and are therefore analogous (Garaba and Zielinski, 2013c).

3.5 Reporting R_{RS} and its uncertainties

Using the herein proposed method, visualization of R_{RS} information can be done as shown Fig. 9. It indicates the average of the four widely used surface reflected glint correction models (Gould et al., 2001; Lee et al., 2010; Mobley, 1999; Ruddick et al., 2006), the range is represented by the maximum and minimum value at each wavelength. Furthermore to numerically present the R_{RS}, Table 2 gives a summary of the information shown in Fig. 9. Although the example provided in Table 1 shows low uncertainties it also provides a way future could present there measurements.

4. Conclusions and Outlook

There are continuing efforts to develop ocean color remote sensing algorithms that are applicable in most water types, with room for improvement, for example to determine inherent optical properties of water GIOP (Werdell et al., 2013). However, in shipborne ocean color remote sensing the challenge of contamination in observations by environmental perturbations namely wind-roughened sea surface contributing to sun glitter and meteorological conditions affects both accuracy and efforts of coming up with common generic methods.

A generic SRG model for shipborne remote sensing is needed due to limited conformity in field observations. Nevertheless, as a recent work summarizes the challenge in developing generic approaches will remain regional and measurement specific (Lee et al., 2014). For example in computing remote sensing reflectance (R_{RS}) from IOPs errors can arise from use of f/Q which is variable ranging between 0.08 – 0.14 and T the reflection and refraction component of water ranging between 0.52 – 0.54 (Aurin and Dierssen, 2012; Li et al., 2013; Loisel and Morel, 2001; Morel and Gentili, 1996). Such flexible variables are an indication that finding a superior model in ocean color remote sensing is complicated but we have to make the best of what we know as well as what field observations and model simulations confirm.

To this end, in this paper we present a modern approach that is reasonably appropriate for automated continuous measurements in shipborne remote sensing. It takes advantage of the commercially available hyperspectral radiometers combined with a camera system for qualitative analysis. In addition, a simple multi-model average SRG correction for remote sensing reflectance (R_{RS}) approach is proposed. Field observations are used to evaluate the usefulness of applying a multi-model averaged R_{RS} in estimating ocean color products. Findings based on used datasets show that to some degree multi-model averaged R_{RS} is reasonably suited for ocean color remote sensing and end-product derivation. Spearman correlation tests confirm our assumption that these four SRG correction models share similarities in there algorithms with very strong significant correlations between G01 and L10 as well as M99 and L06.

The study still has some questions that need to be considered in future investigations; (i) if a surface reflected glint correction approach produces a negative spectrum does it mean the waveband of interest even if positive is wrong?, (ii) is the ± 5 % uncertainty threshold in ocean color applicable when the average of various surface reflected glint correction models is used?, and (iii) what uncertainty or unbiased percent difference threshold would be sufficient to justify use of ‘un-weighted multi-model averaging’? In this work we aim to show a need to have a uniform and traceable methodology to determine R_{RS} and its errors to ensure comparability to future investigations. We also strongly encourage

the ocean color community to submit further field measurements and sufficient matching metadata to open access online repositories like PANGAEA (http://www.pangaea.de/) or SeaBASS (http://seabass.gsfc.nasa.gov/).

We are grateful for the technical support by Rohan Henkel, the captain and crew of the RV Heincke. Financial support by the Coastal Observation System for Northern and Arctic Seas (COSYNA) is appreciated. Radiometric and panoramic images used in study are available on request via email. The helpful comments of two anonymous reviewers are gratefully acknowledged.

References

Aurin, D. A., and Dierssen, H. M., 2012, Advantages and limitations of ocean color remote sensing in CDOM-dominated, mineral-rich coastal and estuarine waters: Remote Sensing of Environment, v. 125, p. 181-197, doi:10.1016/j.rse.2012.07.001.

Barnard, G. A., 1963, New methods of quality control: Journal of the Royal Statistical Society. Series A (General), v. 126, no. 2, p. 255-258, doi:10.2307/2982365.

de Moraes Rudorff, N., Frouin, R., Kampel, M., Goyens, C., Meriaux, X., Schieber, B., and Mitchell, B. G., 2014, Ocean-color radiometry across the Southern Atlantic and Southeastern Pacific: Accuracy and remote sensing implications: Remote Sensing of Environment, v. 149, no. 0, p. 13-32, doi:10.1016/j.rse.2014.03.029.

Draper, D., 1995, Assessment and Propagation of Model Uncertainty: Journal of the Royal Statistical Society. Series B (Methodological), v. 57, no. 1, p. 45-97, doi:10.2307/2346087.

Fougnie, B., Frouin, R., Lecomte, P., and Deschamps, P.-Y., 1999, Reduction of skylight reflection effects in the above-water measurement of diffuse marine reflectance: Applied Optics, v. 38, no. 18, p. 3844-3856, doi:10.1364/AO.38.003844.

Garaba, S., Voß, D., and Zielinski, O., 2014a, Physical, bio-optical state and correlations in North–Western European Shelf Seas: Remote Sensing, v. 6, no. 6, p. 5042-5066, doi:10.3390/rs6065042.

Garaba, S. P., Badewien, T. H., Braun, A., Schulz, A.-C., and Zielinski, O., 2014b, Using ocean colour products to estimate turbidity at the Wadden Sea time series station Spiekeroog: Journal of the European Optical Society, v. 9, p. 14020, doi:10.2971/jeos.2014.14020.

Garaba, S. P., Henkel, R., Krock, B., Voß, D., and Zielinski, O., 2011, Radiance, irradiance, and remote sensing reflectance during the North Sea Coast Harmful Algal Bloom (NORCOHAB II) RV HEINCKE cruise HE302, PANGAEA.

Garaba, S. P., and Zielinski, O., 2013a, Comparison of remote sensing reflectance from above-water and in-water measurements west of Greenland, Labrador Sea, Denmark Strait, and west of Iceland: Optics Express, v. 21, no. 13, p. 15938-15950, doi:10.1364/OE.21.015938.

-, 2013b, Downwelling solar irradiance, upwelling solar radiance, sky leaving radiance, and cloud cover observed during ARCHEMHAB study (on Maria S. Merian Leg MSM21/3) from 2012-07-26 to 2012-08-10, PANGAEA - Data Publisher for Earth & Environmental Science.

Garaba, S. P., and Zielinski, O., 2013c, Methods in reducing surface reflected glint for shipborne above-water remote sensing: Journal of the European Optical Society - Rapid Publications, v. 8, p. 13058, doi:10.2971/jeos.2013.13058.

GCOS, 2011, The Global Climate Observing System - Systematic Observation Requirements for Satellite-based Data Products for Climate: 2011 Update GCOS-154: World Meteorological Organization - Geneva, Switzerland, p. 138.

Gould, R. W., Arnone, R. A., and Sydor, M., 2001, Absorption, scattering, and, remote-sensing reflectance relationships in coastal waters: Testing a new inversion algorithm: Journal of Coastal Research, v. 17, no. 2, p. 328-341,

Harmel, T., Gilerson, A., Tonizzo, A., Chowdhary, J., Weidemann, A., Arnone, R., and Ahmed, S., 2012, Polarization impacts on the water-leaving radiance retrieval from above-water radiometric measurements: Applied Optics, v. 51, no. 35, p. 8324-8340, doi:10.1364/AO.51.008324.

Hodges, J. S., 1987, Uncertainty, policy analysis and statistics: Statistical Science,, v. 2, p. 259-275, doi:10.1214/ss/1177013224.

Hoeting, J. A., Madigan, D., Raftery, A. E., and Volinsky, C. T., 1999, Bayesian model averaging: A tutorial (with comments by M. Clyde, David Draper and E. I. George, and a rejoinder by the authors: Statistical Science, v. 14, no. 4, p. 382-417, doi:10.1214/ss/1009212519.

Hooker, S. B., Lazin, G., Zibordi, G., and McLean, S., 2002, An evaluation of above- and in-water methods for determining water-leaving radiances: Journal of Atmospheric and Oceanic Technology, v. 19, no. 4, p. 486-515, doi: 10.1175/1520-0426(2002)019<0486:AEOAAI>2.0.CO;2

IOCCG, 2008, Why ocean colour? The societal benefits of ocean-colour technology, *in* Platt, T., Hoepffner, N., Stuart, V., and Brown, C., eds., Reports of the International Ocean-Colour Coordinating Group, No. 7: Dartmouth, Canada, p. 147.

Kutser, T., Vahtmäe, E., and Praks, J., 2009, A sun glint correction method for hyperspectral imagery containing areas with non-negligible water leaving NIR signal: Remote Sensing of Environment, v. 113, no. 10, p. 2267-2274, doi:10.1016/j.rse.2009.06.016.

Lee, Z., Ahn, Y.-H., Mobley, C., and Arnone, R., 2010, Removal of surface-reflected light for the measurement of remote-sensing reflectance from an above-surface platform: Optics Express, v. 18, no. 25, p. 26313-26324, doi:10.1364/OE.18.026313.

Lee, Z., Shang, S., Hu, C., and Zibordi, G., 2014, Spectral interdependence of remote-sensing reflectance and its implications on the design of ocean color satellite sensors: Applied Optics, v. 53, no. 15, p. 3301-3310, doi:10.1364/AO.53.003301.

Li, L., Li, L., Song, K., Li, Y., Tedesco, L. P., Shi, K., and Li, Z., 2013, An inversion model for deriving inherent optical properties of inland waters: Establishment, validation and application: Remote Sensing of Environment, v. 135, p. 150-166, doi:10.1016/j.rse.2013.03.031.

Loisel, H., and Morel, A., 2001, Non-isotropy of the upward radiance field in typical coastal (Case 2) waters: International Journal of Remote Sensing, v. 22, no. 2-3, p. 275-295, doi:10.1080/014311601449934.

Makridakis, S., 1993, Accuracy measures: theoretical and practical concerns: International Journal of Forecasting, v. 9, no. 4, p. 527-529, doi:10.1016/0169-2070(93)90079-3.

Mobley, C. D., 1999, Estimation of the remote-sensing reflectance from above-surface measurements.: Applied Optics, v. 38, no. 36, p. 7442-7455, doi:10.1364/AO.38.007442.

Moore, G. K., 1980, Satellite remote sensing of water turbidity / Sonde de télémesure par satellite de la turbidité de l'eau: Hydrological Sciences Bulletin, v. 25, no. 4, p. 407-421, doi:10.1080/02626668009491950.

Morel, A., and Gentili, B., 1996, Diffuse reflectance of oceanic waters. III. Implication of bidirectionality for the remote-sensing problem: Applied Optics, v. 35, no. 24, p. 4850-4862, doi:10.1364/AO.35.004850.

Mueller, J. L., Davis, C., Arnone, R., Frouin, R., Carder, K., Lee, Z. P., Steward, R. G., Hooker, S., Mobley, C. D., and McLean, S., 2003, Above-Water Radiance and Remote Sensing Reflectance Measurement and Analysis Protocols, *in* Mueller, J. L., Fargion, G. S., and McClain, C. R., eds., Radiometric Measurements and Data Analysis Protocols Ocean Optics Protocols For Satellite Ocean Color Sensor Validation, Revision 4, Volume III: Greenbelt, Maryland, p.

Nakagawa, S., and Freckleton, R., 2011, Model averaging, missing data and multiple imputation: a case study for behavioural ecology: Behavioral Ecology and Sociobiology, v. 65, no. 1, p. 103-116, doi:10.1007/s00265-010-1044-7.

Olszewski, J., and Darecki, M., 1999, Derivation of remote sensing reflectance of Baltic waters from above-surface measurements: Oceanologia, v. 41, no. 1, p. 99-111,

Olszewski, J., and Kowalczuk, P., 2000, Sky glint correction in measurements of upward radiance above the sea surface: Oceanologia, v. 42, no. 2, p. 251–262,

Pegau, W. S., Gray, D., and Zaneveld, J. R. V., 1997, Absorption and attenuation of visible and near-infrared light in water: dependence on temperature and salinity. Appl. Opt., v. 36, p. 6035-6046,

Röttgers, R., McKee, D., and Wozniak, S. B., 2013, Evaluation of scatter corrections for ac-9 absorption measurements in coastal waters: Methods in Oceanography, v. 7, p. 21-39, doi:10.1016/j.mio.2013.11.001.

Ruddick, K. G., De Cauwer, V., Park, Y. J., and Moore, G., 2006, Seaborne measurements of near infrared water-leaving reflectance: The similarity spectrum for turbid waters: Limnology and Oceanography, v. 51, no. 2, p. 1167-1179,

Tanaka, A., Sasaki, H., and Ishizaka, J., 2006, Alternative measuring method for water-leaving radiance using a radiance sensor with a domed cover: Optics Express, v. 14, no. 8, p. 3099-3105, doi:10.1364/OE.14.003099.

Toole, D. A., Siegel, D. A., Menzies, D. W., Neumann, M. J., and Smith, R. C., 2000, Remote-sensing reflectance determinations in the coastal ocean environment: Impact of instrumental characteristics and environmental variability: Applied Optics, v. 39, no. 3, p. 456-469, doi:10.1364/AO.39.000456.

Wang, P., Boss, E. S., and Roesler, C., 2005, Uncertainties of inherent optical properties obtained from semianalytical inversions of ocean color: Applied Optics, v. 44, no. 19, p. 4074-4085, doi:10.1364/AO.44.004074.

Werdell, P. J., Franz, B. A., Bailey, S. W., Feldman, G. C., Boss, E., Brando, V. E., Dowell, M., Hirata, T., Lavender, S. J., Lee, Z., Loisel, H., Maritorena, S., Mélin, F., Moore, T. S., Smyth, T. J., Antoine, D., Devred, E., d'Andon, O. H. F., and Mangin, A., 2013, Generalized ocean color inversion model for retrieving marine inherent optical properties: Applied Optics, v. 52, no. 10, p. 2019-2037, doi:10.1364/AO.52.002019.

Yan, Y., and Sydor, M., 2006, Surface corrections for remote sensing reflectance in Case 2 waters of Lake Superior: Journal of Great Lakes Research, v. 32, no. 3, p. 407-414, doi:10.3394/0380-1330(2006)32[407:SCFRSR]2.0.CO;2.

436 **Table 1** Statistical results from comparison analysis between in-water derived remote sensing reflectance
437 (R_{RS}) and above-water derived R_{RS}. M(A)PD is the mean (absolute) percent difference ± standard
438 deviation.

Wavelength [nm]	M99	G01	R06	L10	Average
440 - MPD	-24 ± 47	-9 ± 45	-25 ± 48	3 ± 47	-25 ± 45
440 – MAPD	48 ± 21	40 ± 22	49 ± 21	40 ± 24	46 ± 22
488 – MPD	-9 ± 44	0 ± 42	-8 ± 44	3 ± 48	-14 ± 46
488 – MAPD	39 ± 22	36 ± 20	39 ± 22	42 ± 23	42 ± 22
555 – MPD	-12 ± 43	5 ± 45	-12 ± 44	-1 ± 45	-2 ± 48
555 – MAPD	40 ± 21	39 ± 23	40 ± 21	38 ± 24	42 ± 22
676 – MPD	-8 ± 43	8 ± 39	-8 ± 42	-10 ± 43	-10 ± 44
676 – MAPD	37 ± 22	34 ± 21	37 ± 22	39 ± 20	39 ± 23
715 – MPD	-18 ± 44	8 ± 42	-19 ± 43	-4 ± 41	-5 ± 45
715 – MAPD	42 ± 22	36 ± 21	41 ± 22	35 ± 21	41 ± 20
488/555 - MPD	-7 ± 32	6 ± 35	-6 ± 34	6 ± 36	3 ± 32
488/555 - MAPD	24 ± 22	29 ± 21	27 ± 22	30 ± 22	26 ± 20

439

440

441 Table 2 Remote sensing reflectance (R_{RS}) on 12 March 2013 at 10:00 from the port side aboard R/V
442 Heincke.

Wavelength [nm]	R_{RS} [$\times 10^{-3}$ sr^{-1}]	Min R_{RS} [$\times 10^{-3}$ sr^{-1}]	Max R_{RS} [$\times 10^{-3}$ sr^{-1}]	UPD [%]	Max Error [$\times 10^{-4}$ sr^{-1}]
410	5.139	4.942	5.318	7.33	1.88
440	7.299	7.048	7.443	5.44	1.97
490	11.016	10.705	11.195	4.47	2.45
510	11.269	10.942	11.458	4.61	2.58
555	11.019	10.663	11.224	5.13	2.80
645	3.214	2.825	3.439	19.60	3.07

Fig. 1. The camera system highlighted in yellow onboard R/V Heincke.

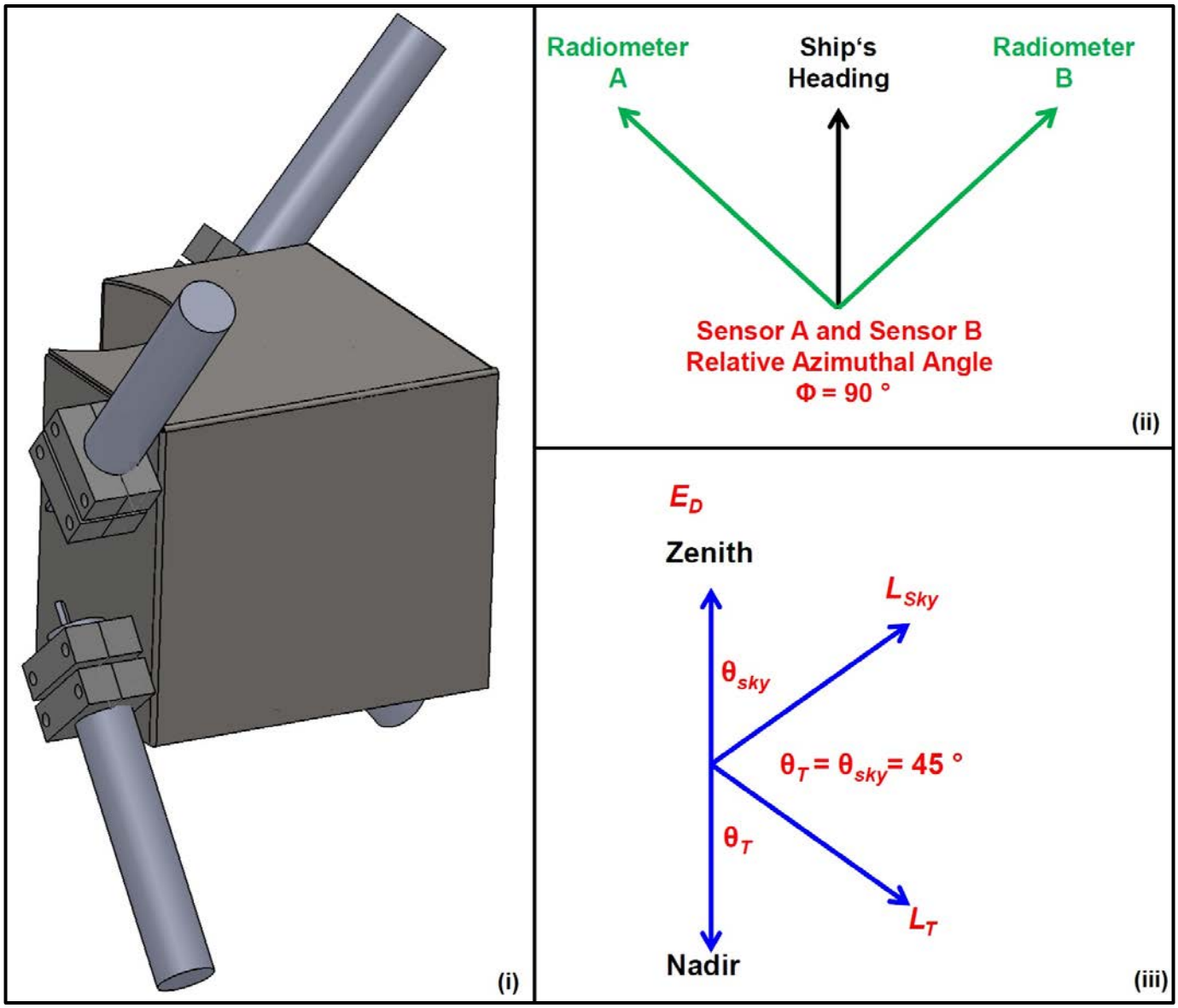

Fig. 2. A schematic of the radiometer setup onboard the R/V Heincke. (i) is the model of the radiometers and the platform, (ii) a top view of the radiometers, and (iii) a side view of the radiometer geometry.

450

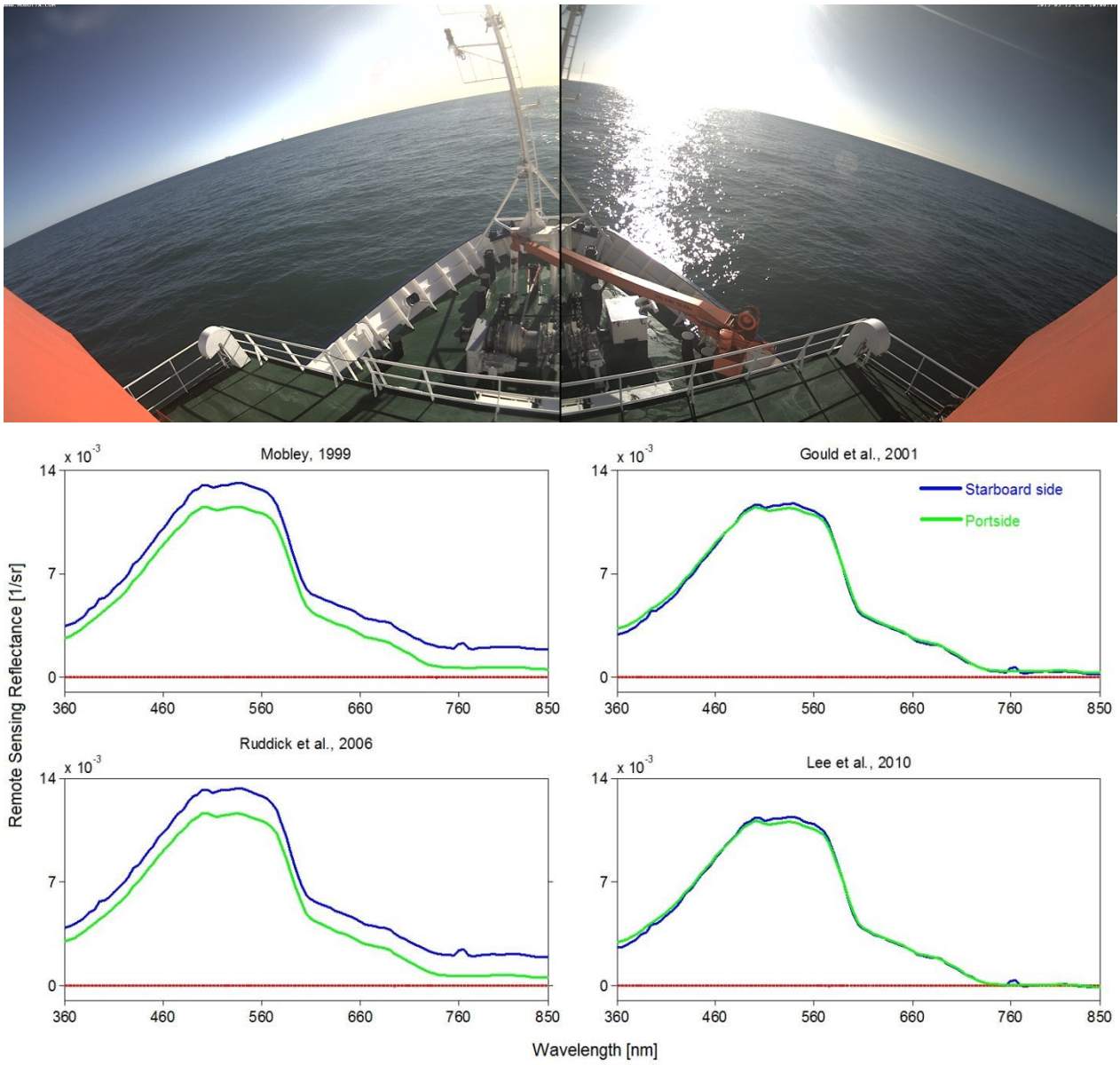

451

452

453 Fig. 3. An example of sea surface and sky images collected onboard R/V Heincke with the matching
454 surface reflected glint corrected R_{RS} spectra on 12 March 2013 at 10:00. Red line indicates the zero
455 reflectance line.

456

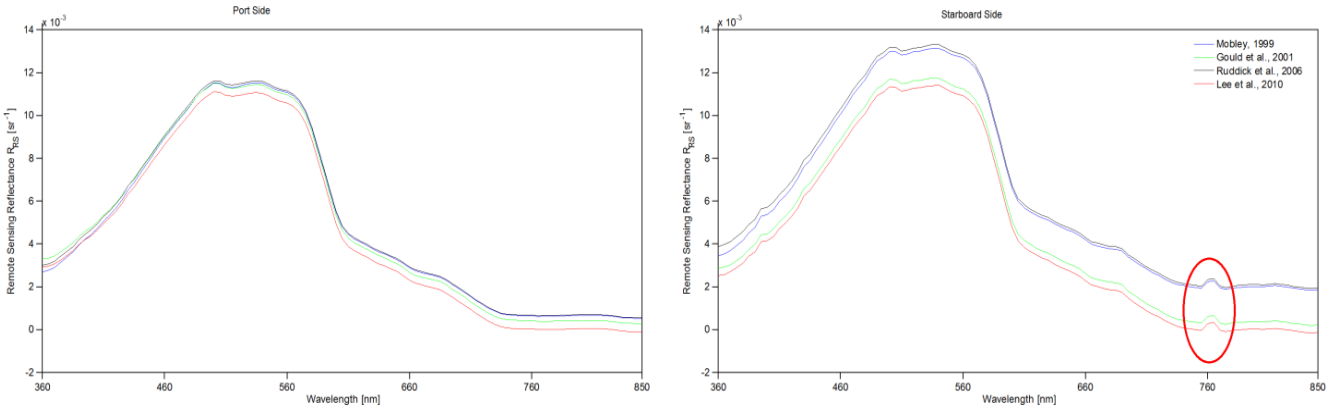

Fig. 4. Example of a surface reflected glint correct Remote sensing reflectance (R_{RS}) spectra on 12 March 2013 at 10:00 aboard R/V Heincke. The highlighted red part indicates a peak around 760 nm observed in spectra strongly influenced by surface reflected glint.

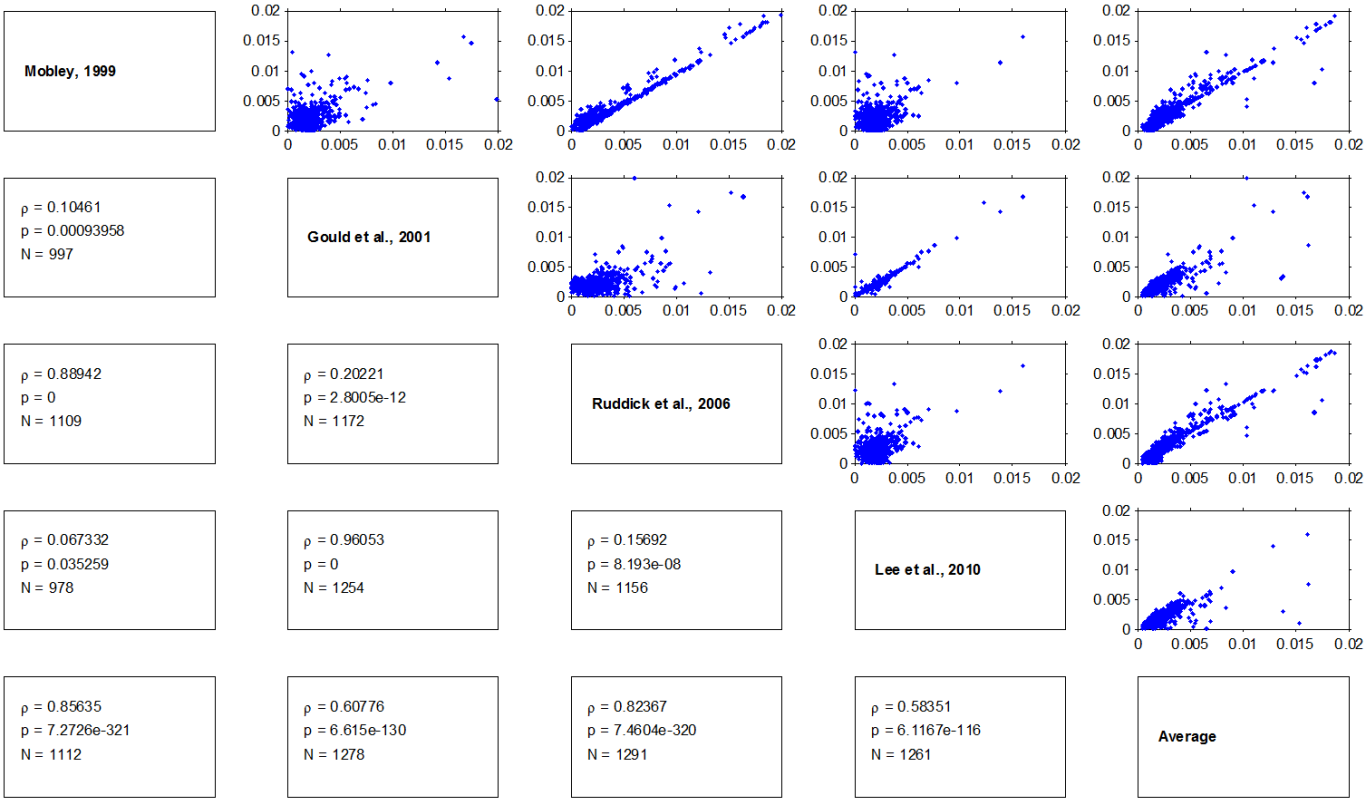

Fig. 5. Spearman's rank-order correlation statistics at 440 nm for measurements from high latitude melt waters and fjordal waters as well as northwestern European shelf seas.

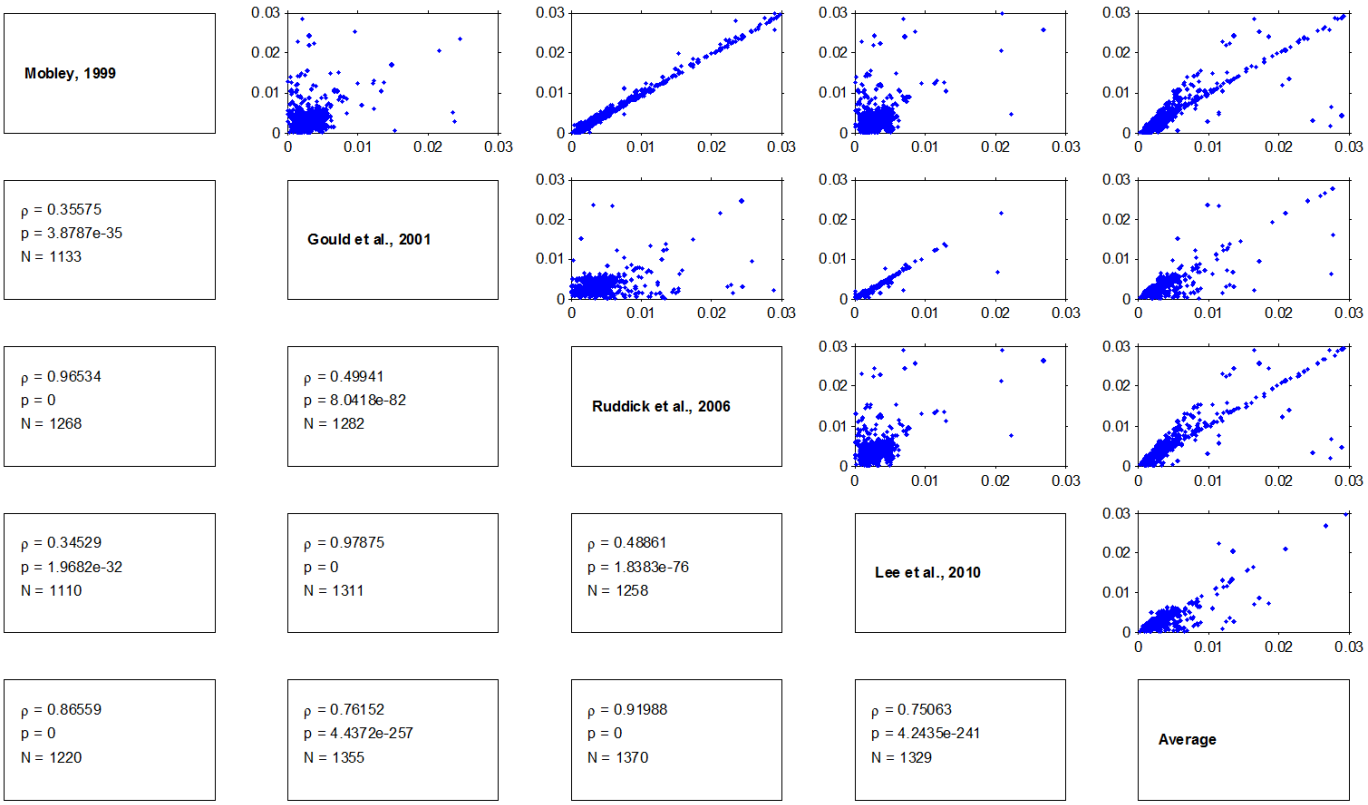

Fig. 6. Spearman's rank-order correlation statistics at 555 nm measurements from high latitude melt waters and fjordal waters as well as northwestern European shelf seas.

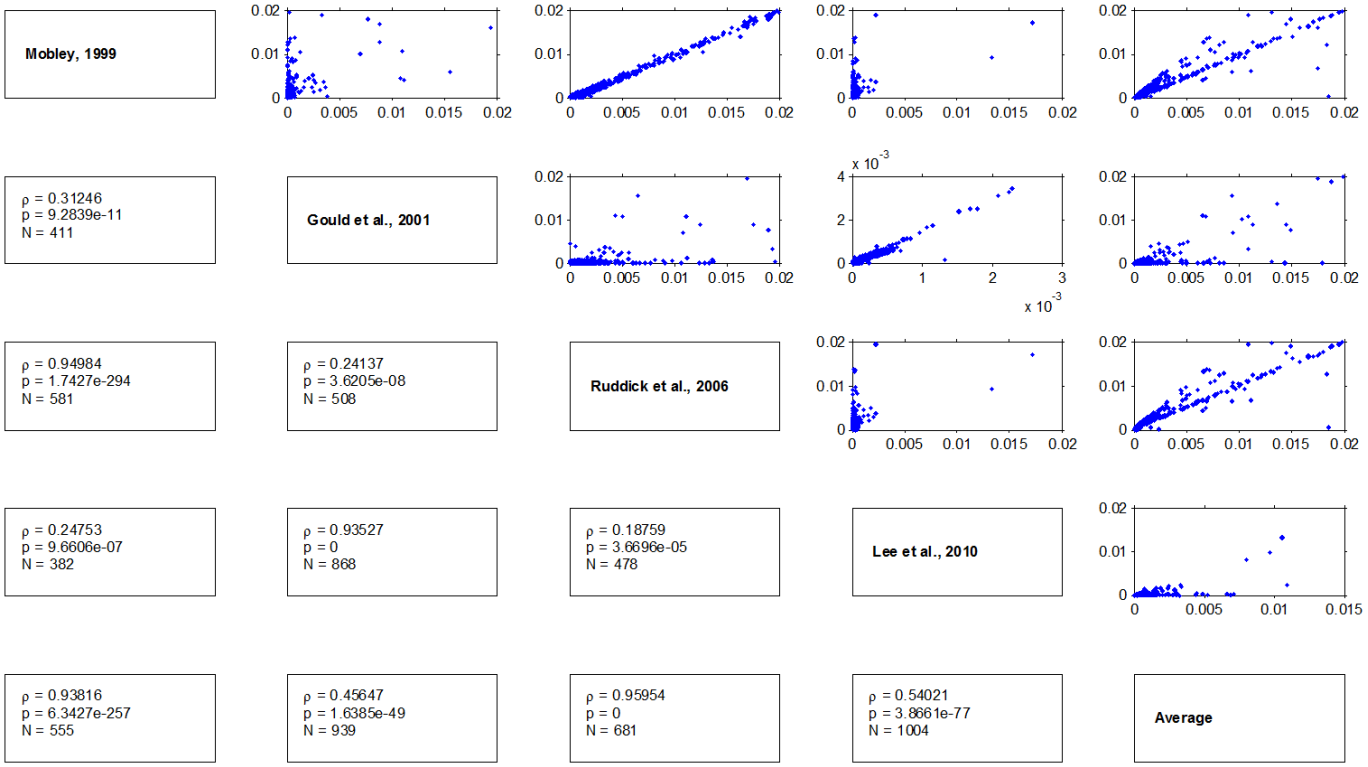

471 Fig. 7. Spearman's rank-order correlation statistics at 715 nm measurements from high latitude melt
472 waters and fjordal waters as well as northwestern European shelf seas.
473

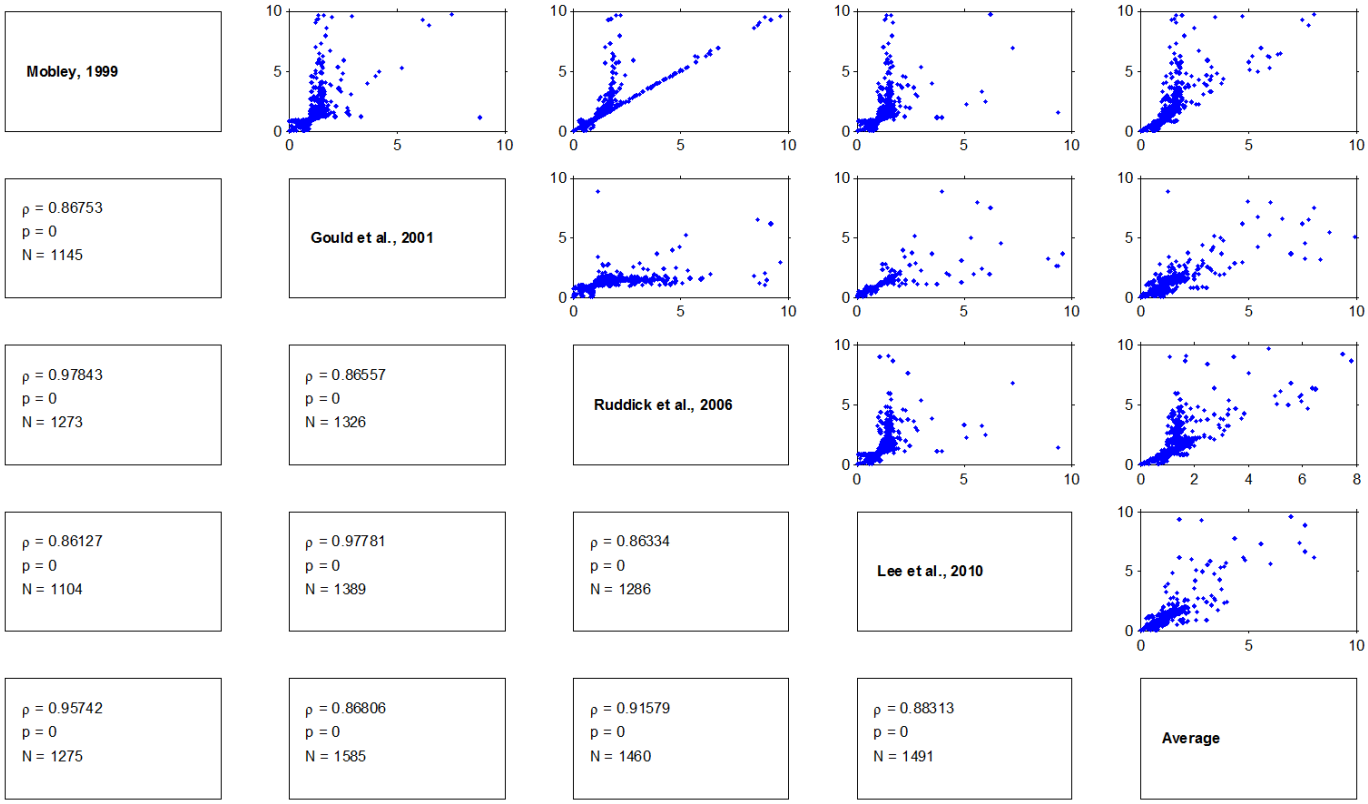

474

475 Fig. 8. Spearman's rank-order correlation statistics at (490/555) nm measurements from high latitude
476 melt waters and fjordal waters as well as northwestern European shelf seas.

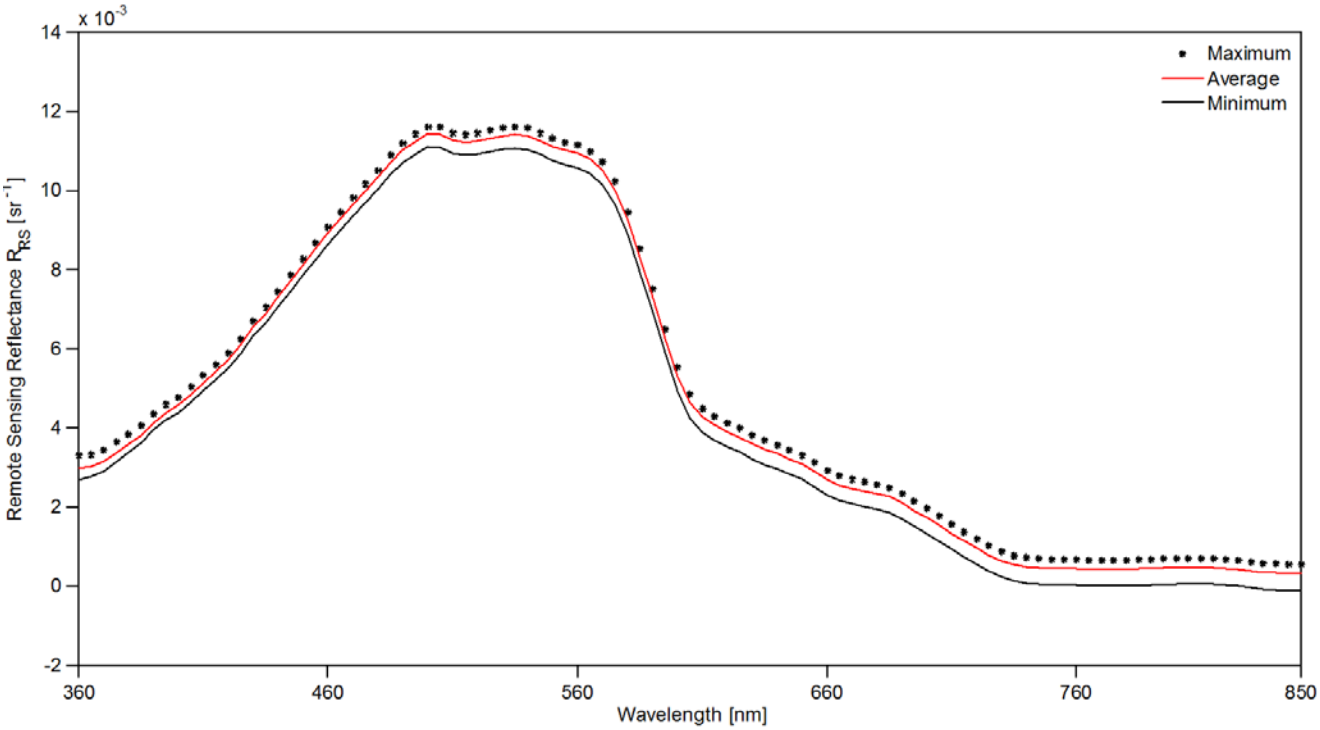

477

Fig. 9. Example of a surface reflected glint correct R_{RS} spectra on 12 March 2013 at 10:00 from the port side aboard R/V Heincke.